Egypt. J. Chem. **Vol. 67,** No. 4 pp. 45 - 54 (2024)

Egyptian Journal of Chemistry

http://ejchem.journals.ekb.eg/

Preparation and Characterisation of $Ca_3Co_{4-X}Cu_XO_9$ ($0 \leq X \leq 0.3$) as Cathode Materials for Intermediate Temperature Solid Oxide Fuel Cell (SOFC)

Hussien A. Abbas*

Inorganic Chemistry Department, National Research Centre, El Behouth Street Dokki, Cairo, 12622, Egypt

Abstract

Intermediate temperature solid oxide fuel cells (IT-SOFC) working at 600-800 °C attracted considerable attention as compared to the traditional SOFCs as highly clean efficient power generation source. In this frame this paper focuses on the preparation and characterization of Ca3Co4-xCuxO9 (x=0, 0.1, 0.2 and 0.3) as cathode material for IT-SOFC. Ca3Co4-xCuxO9 (x=0, 0.1, 0.2 and 0.3) powders were prepared using the Pechini method. The effect of Cu doping on the crystal structures of Ca3Co4O9 were investigated using x-ray diffraction (XRD). Ca3Co4O9, Ca3Co3.9Cu0.1O9 and Ca3Co3.8Cu0.2O9 samples have a similar crystal structure of that reported for Ca3Co4O9 indicating monoclinic phase compounds whereas Ca3Co3.7Cu0.3O9 sample has orthorhombic CaCuO2 as a minor phase and a monoclinic Ca3Co4O9 as a major phase. The sinterability of Ca3Co4O9, Ca3Co3.9Cu0.1O9 and Ca3Co3.8Cu0.2O9 samples was studied. The effects of sintering time and temperature on the microstructure, homogeneity of the prepared electrodes and the adhesion to an anode supported cell were studied using scanning electron microscopy (SEM). The effect of ball milling time on the particle size distribution of the prepared samples was reported. The electrochemical properties of Cu-CCO-GDC composite cathodes were studied. The lowest area specific resistance was obtained for 50 wt% GDC-50 wt% Ca3Co3.8Cu0.2O9 composite cathode showing that it could be a promising cathode material for IT-SOFC.

Keywords: Ca3Co4O9; Cu doping; SOFC; Cathode materials; microstructure

1. Introduction

The research in Solid Oxide Fuel Cells (SOFC) aims to diminish the working temperature to intermediate temperature range (500-700 °C) to diminish the running expenses, to enhance the materials compatibility, to reduce the time for startup and to acquire long time durability [1–3]. However, the decrease of the operating temperature results in increasing the electrolyte ohmic losses and also decreasing the electrocatalytic activity at the cathode which in turn results in decreasing the electrochemical performance at the cathode [4,5].

There are many interests at present in improving the electrochemical performance of the cathode by finding new cathode materials for intermediate temperature Solid Oxide Fuel Cells (IT-SOFC). The state of the art SOFC cathode materials are the perovskite (La,Sr)(Co,Fe)O_3 (LSCF), (La,Sr)CoO_3 (LSC), (La,Sr)MnO_3 (LSM), and (La,Sr)FeO_3. These materials have good catalytic activity for oxygen reduction, high oxide ion conductivity, and high electronic conductivity. Among these cathodes, the major drawbacks of the cobalt based oxides are the chemical and thermal expansion compatibilities with the standard electrolytes such as yttrium doped zirconia (YSZ), gadolinium doped ceria (GDC) or $La_{1-x}Sr_xGa_{1-y}Mg_yO_3$ (LSGM) [6]. Other structures have been suggested to reduce the thermal expansion coefficient (TEC), among them are perovskites, layered perovskites [7] and layered Ruddlesden-Popper phases $A_{n+1}B_nO_{3n+1}$ (A=rare earth/alkaline earth; B=transition metal), such as (La, Sr)$_{n+1}$(Fe,Co)$_n$O$_{3n+1}$ [8].

*Corresponding author e-mail: hu_abbas2005@yahoo.com.; (H. A. Abbas).
Receive Date: 05 March 2023, Revise Date: 05 October 2023, Accept Date: 22 October 2023
DOI: 10.21608/EJCHEM.2023.197881.7685

The well-known thermoelectric material, $Ca_3Co_4O_9$ (CCO), is one of the candidates that could be used as a cathode for IT-SOFC because its thermal expansion coefficient is well matched with that of GDC; it has also good compatibility with GDC and it also has good chemical durability [6,9]. Several authors were interested in improving the thermoelectric properties of CCO [10–17]. However, few studies are found on the electrochemical performance of CCO as a cathode for IT-SOFC. Nagasawa et al [6] have prepared CCO and studied its structure, chemical, mechanical adaptability and electrochemical performance as a candidate for IT-SOFC. For improving the CCO electrochemical performance, A. Rolle et al [18] have investigated the effect of several parameters on the cathode performance such as pore former, electrolyte and cathode composition. Moreover, A. Rolle et al [19] have investigated the effect of current collectors. Yehia et al [20] have synthesized and evaluated $Ca_{3-x}La_xCo_4O_{9+\delta}$ as cathode material for proton conducting fuel cells. The lowest polarization resistance (Rp=0.64 $\Omega.cm^2$ at 600 °C) have been obtained by Samson et al [9] for 40 wt%CCO-60wt% $Gd_{0.1}Ce_{0.9}O_2$ composition. Recently, Zou et al have prepared and evaluated $Ca_{3-x}Bi_xCo_4O_{9-\delta}$ as cathode material for IT-SOFC [21]. Also, Zou et al [22] have studied the effect of transition metal ions dopants on the electrochemical performance of $Ca_{2.9}Bi_{0.1}Co_4O_{9-\delta}$ cathode. Guo et al [23] have studied composite of 50 wt% CCO and 50 wt% $La_{0.7}Sr_{0.3}CoO_3$ as a candidate material for IT-SOFC cathode. The electrochemical properties and the transport properties of CCO and Sr, Bi, Pb and La-doped CCO have been presented by Mignardi [23]. Thoreton et al. [24] have studied the oxide ion diffusion and the kinetics for the oxygen transfer at the surface of CCO where it was found that at 700 °C, the diffusion coefficient (D*) is $2.7.10^{-10}$ $cm^2.s^{-1}$ and the surface exchange coefficient (K*) is $1.6.10^{-7}$ $cm.s^{-1}$. The good ionic and electronic conduction of CCO makes it fascinating cathode material for SOFC. Other studies for improving the performance of CCO as cathode material have been found [21,23,25–28]. Several authors were interested in improving the thermoelectric properties of CCO by Cu doping [29–32]. The Cu-doping at Co-site induces a significant decrease of the resistivity for CCO while the electronic correlation almost remains unchanged [30]. On the foregoing literature survey, Cu-doped CCO system is not evaluated as IT-SOFC cathode. The aim of the present work is the preparation and characterization of Cu-doped CCO with special interest in the investigation of the influence of Cu concentration systematically on the structural, microstructural, shrinkage and the electrochemical properties of CCO to be used as a cathode for SOFC.

2. Materials and Methods

2.1. Materials

$Ca_3Co_4O_9$ was prepared using polymeric precursor route based on Pechini method [33] which had been used in the preparation of many metal oxides [34,35]. $Ca(NO_3)_2.4H_2O$ (99-103%, Alfa), $Co(NO_3)_2.6H_2O$ (99%, Merck), $Cu(NO_3)_2.3H_2O$ (99.5 %, Alfa), $C_6H_8O_7.H_2O$ (99.5-100.5%, Merck) and $C_2H_4(OH)_2$ (99.5%, Merck) were used as starting materials.

2.2. Sample Preparation

Aqueous cobalt nitrate and calcium nitrate solutions were mixed, considering the desired stoichiometry of the metal oxides in the final ceramic powder. Citric acid (CA) was then added to chelate metal cations at the CA:cations molar ratio of 4:1. After dissolving the CA, ethylene glycol (EG) was added into the solution at CA:EG molar ratio of 1:1.5. The solution was stirred for 30 minutes for homogenization and heated up to 100 ºC and kept under stirring until a gel was formed. Then the temperature is increased gradually up to 300 °C. The charred gel is heated in air in a muffle furnace at 200 °C for 2 h and then at 600 °C for 2 h. The resulted black foam is heated at 800 °C for 5 h in air and the resulting powder was milled using a planetary ball mill (Retsch, PM 400) for 15 minutes. Fig. 1 shows the flow chart of the preparation of $Ca_3Co_4O_9$. $Ca_3Co_{4-x}Cu_xO_9$ powder samples (x=0.1, 0.2 and 0.3) were prepared using the same method.

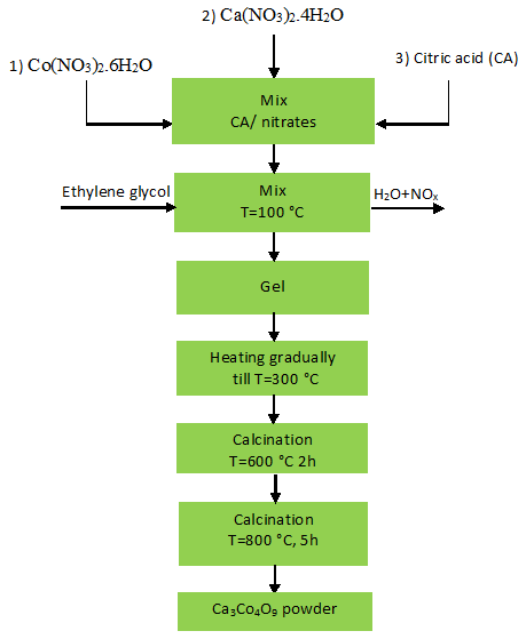

Fig. 1 Flow chart for the preparation of $Ca_3Co_4O_9$ powder.

2.3. Sample Characterizations

Chemical analysis was performed on the previously prepared samples to adjust the stoichiometry on Agilent 5100 Inductively Coupled Plasma – Optical Emission Spectrometer (ICP-OES) with Synchronous Vertical Dual View (SVDV). It was found that all samples possess the calculated amount of Co, Ca and Cu. The phase compositions for all the prepared samples were identified using X-ray diffraction (XRD) using (Bruker, D4) with Cu-Kα radiation at room temperature. The particle size distribution was measured using (Retsch, LA-950). The sinterability was measured using (Netzsch, DIL-402C) dilatometer from room temperature to 800 °C for CCO and from room temperature to 850 °C and to 900 °C for all the prepared samples in air with a heating rate of 5 °C/min. For the preparation of CCO ink, 23.5 wt % of ethyl cellulose-terpineol was added to CCO sample and terpineol was added to adjust the viscosity then the mixture was homogenized by the three roll mill (Exakt 80E, Germany). The same method of ink preparation was applied for all the CCO based samples and for 50wt% $Ca_3Co_4O_9$-50wt% $Gd_{0.2}Ce_{0.8}O_2$ (x_0-GDC), 50 wt% $Ca_3Co_{3.9}Cu_{0.1}O_9$-50 wt% $Gd_{0.2}Ce_{0.8}O_2$ ($x_{0.1}$-GDC), 50wt % $Ca_3Co_{3.8}Cu_{0.2}O_9$-50 wt % $Gd_{0.2}Ce_{0.8}O_2$ ($x_{0.2}$-GDC) composite cathodes. The ink was screen printed on anode supported cells. The cathodes were dried at 60 °C in air for about 1 h. To study the effect of sintering time on the cathodes microstructures, x=0-0.1 cathodes were sintered at 500 °C for 1 h then at 900 °C for different sintering time (3, 4 and 5 h). X=0.1-0.2 cathodes because of stability reasons were sintered at 500 °C for 1 h then 850 °C for different sintering time (2, 3, 4, and 5 h). The cross-section microstructure of all the sintered cathodes was characterized by (Hitachi, TM-1000) scanning electron microscope. Impedance spectroscopy measurements were performed using the Solartron, SI 1260 analyzer in the 1.0 mHz-1.0 MHz domain. The imposed signal amplitude during measurements was verified to be low enough (50 mV) for a zero DC polarization current approximation, with respect to the linearity of the electrical response. Gold electrodes were used as current collectors. Measurements were performed in air from 600 to 800 °C.

3. Results and discussion

3.1. X-ray diffraction

The XRD patterns of $Ca_3Co_{4-x}Cu_xO_9$ (x=0, 0.1, 0.2 and 0.3) samples prepared by pechini method are shown in Fig. 2. X=0-0.2 samples agree well with the JCPDS (21-139) and the reported data for $Ca_3Co_4O_9$ [36,37] indicating monoclinic phase compounds whereas traces of additional orthorhombic phase of $CaCuO_2$ were detected for x=0.3 sample. It can be observed that the diffraction peaks slightly shifted towards lower theta value as the concentration of Cu increases until the x=0.2 sample. The shift in the diffraction peaks might be due to the difference in the ionic radii between Cu ions and Co ions. In the Cu-doped $Ca_3Co_4O_9$ system, the Cu ions might substitute Co ions in CoO_2 layers or in the Ca_2CoO_3 layers. The standard ionic radius of Cu^{2+} ion is 0.73 Å whereas the ionic radius is 0.545 Å for Co^{3+} ion in CoO_2 layers and is 0.745 Å for Co^{2+} ion in Ca_2CoO_3 layers. Accordingly, Cu^{2+} ions will substitute Co^{2+} ions in Ca_2CoO_3 layers [30].
The shift in the diffraction peaks of x=0.2 sample is similar to that of x=0.3 sample. This might be attributed to Cu ions substituting Co ions like x=0.2 sample and the excess of Cu ions form $CaCuO_2$ phase. The average crystallite size was calculated for all the sample using Scherrer Equation (1):

$$L=\frac{K\lambda}{\beta\cos\theta} \qquad (1)$$

Where L is the average crystallite size, λ is the wavelength of the used x-ray, K=0.9, β is the full width at half maximum intensity (FWHM), 2θ is peak position. The calculated average crystallite size was presented in Table 1. Cu doping resulted in increase in the average crystallite size.

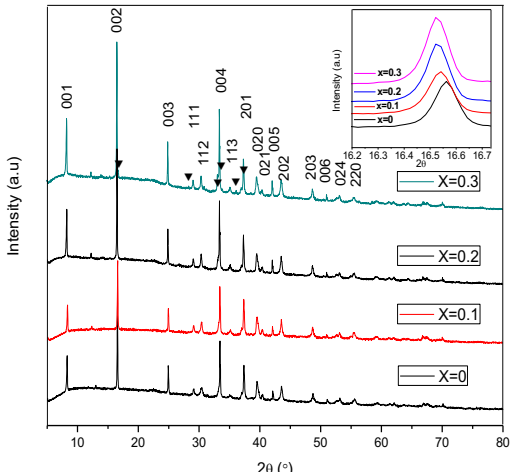

Fig. 2 X-ray diffractograms of the prepared samples. ▼symbol represents the orthorhombic phase of $CaCuO_2$.

Table 1

The average crystallite size of the prepared samples.

Sample	Average crystallite size (nm)
X=0	71
X=0.1	73
X=0.2	74
X=0.3	75

3.2. Sinterability

Due to the XRD-analysis which shows that x=0.3 sample is composed of a mixture of phases, samples x=0-0.2 were selected for further experiments.

The thermal expansion coefficient of both $Ca_3Co_4O_9$ (CCO) and 70 wt % CCO-30 wt % GDC have been reported by Nagasawa et al [6]. Dilution of CCO by 30 mole % GDC slightly shifted its expansion coefficient form 9-10 x 10^{-6} $°C^{-1}$ to 10-11 x 10^{-6} $°C^{-1}$ and interestingly, both of them are matched well with that of the standard GDC electrolyte (~10x10^{-6} $°K^{-1}$).

$Ca_3Co_4O_9$ crystallizes in a monoclinic elementary cell, which is divided in two sublattices: sublattice H which is the hexagonal Cd-I_2 type layers [CoO_2] and sublattice RS which is the rock salt blocks [$Ca_2CoO_{3-\delta}$]. Both sublattices have the same lattice parameters a and c but differ in the b lattice parameter where b_H is b lattice parameter for sublattice H whereas b_{RS} is b lattice parameter for sublattice RS [6]. Nagasawa et al [6] performed HT-XRD experiments to evaluate the anisotropy of the thermal expansion along the distinct crystallographic axes. It is found that the lattice parameters a, b_H and c increases as the temperature increases till 775 °C. At this temperature, a change of the slope is detected which is attributed to the change in the cobalt spin state. The lattice parameter b_{RS} is found to be nearly constant as the temperature increases. The cobalt electronic configuration changes from Co^{3+} to Co^{4+} within the Cd-I_2 layers as deduced from the change in the slope of a, b_H and c in addition to the less temperature dependence of b_{RS}.

The same trend of linear thermal expansion ($\Delta L/L_0$) as a function of temperature detected by Nagasawa et al [6] for CCO was detected for our prepared samples (CCO, Cu-doped CCO samples) when the samples are heated up to 800 °C, 850 °C and 900 °C where ($\Delta L/L_0$) increases as the temperature increases (Figs.3-4).

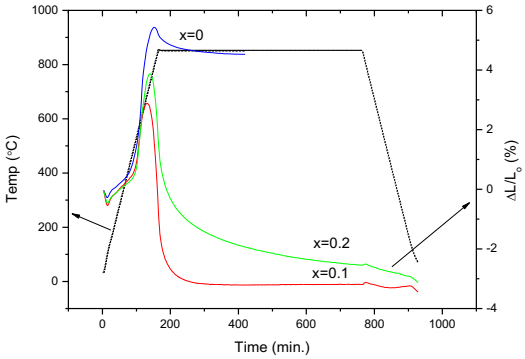

Fig. 3 Sinterability of $Ca_3Co_{4-x}Cu_xO_9$ (x=0-0.2 samples) after dilatometry at 850 °C/10 h as a function of temperature and time.

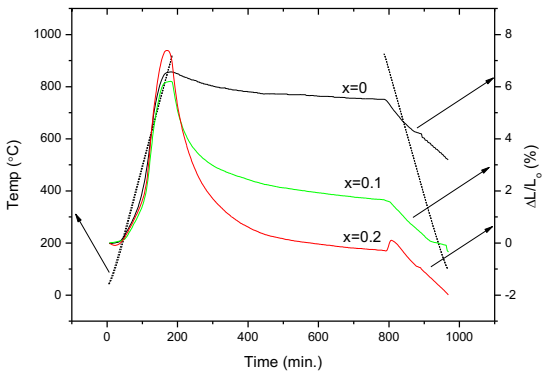

Fig. 4 Sinterability of $Ca_3Co_{4-x}Cu_xO_9$ (x=0-0.2 samples) after dilatometry at 900 °C/10 h as a function of temperature and time.

From Figs. 3-4, it is clear that there is no sinterability shrinkage observed for x=0 sample at 800 °C and 850 °C. There is slight improving in the sinterability shrinkage of x=0 sample at 900 °C. This could be attributed to progressive oxygen loss which is in agreement to Oide et al [38] where on heating in air at 900 °C, progressive oxygen loss is detected and δ is about 0.01. From Fig. 3 it was found that Cu doping reduces the temperature at which the shrinkage starts to take place and also the shrinkage is higher for Cu-doped samples than the undoped CCO. x=0.1 sample (10 mole % Cu-doped CCO sample), the rate of shrinkage is higher than that of undoped CCO. This might be due to Cu segregates at the grain boundaries and improve the diffusivity of ions increasing the density. No shrinkage was detected for x=0.1 sample after about 300 min. The rate of shrinkage of x=0.2 sample is lower than x=0.1 sample. XRD at room temperature was performed to detect the crystal structure of the samples after dilatometry up to 850 °C (Fig. 5). No phase transformation or decomposition was detected for all the samples after cooling at room temperature. Better crystallinity was detected for all the samples after dilatometry experiments up to 850 °C.

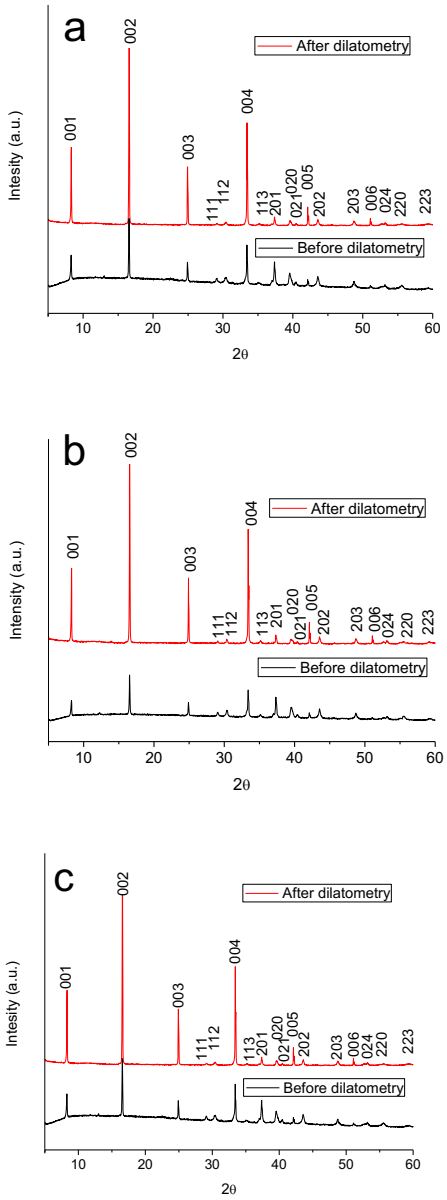

Fig. 5 XRD patterns of a)x=0, b)x=0.1 and c)x=0.2 samples performed before and after dilatometry tests carried out up to 850 °C/10 h.

At 900 °C (Fig. 4), the rate of shrinkage of the x=0.1 is higher than that of the undoped CCO sample. Moreover, the rate of shrinkage of x=0.1 sample is lower than that of x=0.2. No phase transformation or decomposition was detected for the undoped CCO or x=0.1 samples after the dilatometry tests (Fig. 6). Unfortunately, the x=0.2 sample decomposed during sintering at 900°C where traces of additional phases such as the

rhombohedral phase of $Ca_3Co_2O_6$, orthorhombic phase of $Cu_{64}O$, and hexagonal phase of $CoO_{1.92}$ phases were detected (Fig. 7).

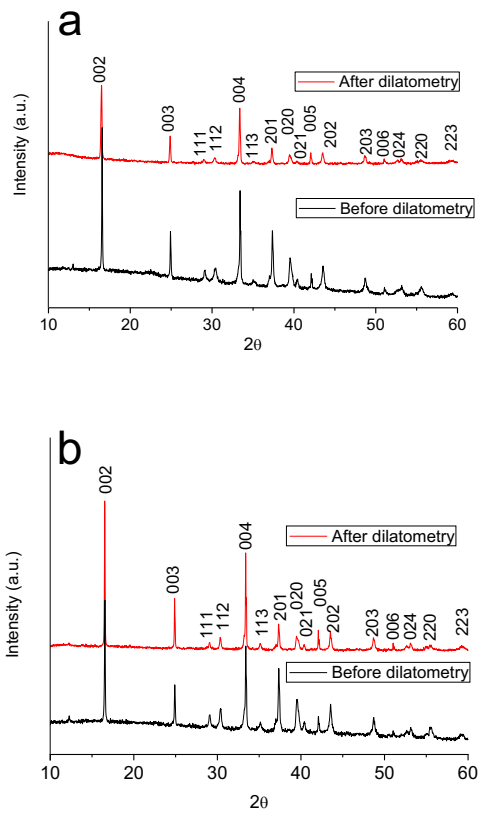

Fig. 6 XRD patterns of a) x=0, b) x=0.1 samples performed before and after dilatometry tests carried out up to 900 °C/10 h.

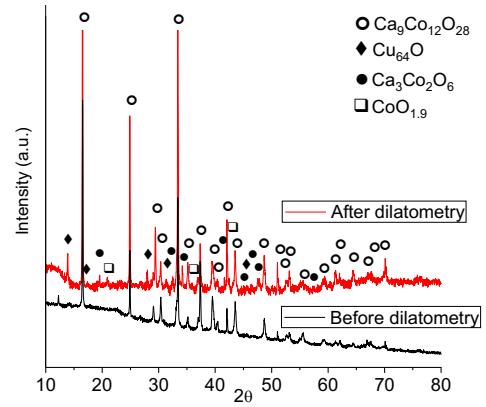

Fig. 7 XRD patterns of x=0.2 sample before and after dilatometry tests up to 900 °C/10 h.

3.3. Particle size distribution

After Pechini´s method preparation, it was found that all the particles appeared to have strong agglomeration and there are two particle size distributions observed and some of the grains have size higher than 100 µm (Fig. 8a). The particle size (d_{50}) was determined to be 9.55 µm for x=0 sample after the Pechini´s method of preparation. For improving the screen printability, the powders were ball milled for various durations to reduce the grain size. It was found that after ball milling of the x=0 sample for 2 h in ethanol using a roller bench mill, a unimodal particle size distribution in the range of about 1 to 10 µm was observed and the particle size d_{50} was determined to be 4.6 µm (Fig 8 b). After ball milling for 8 h, a bimodal distribution was observed and the particle size d_{50} was determined to be 3.86 µm (Fig. 8c). After ball milling for 16 and 40 h, there is no valuable reduction in the particle size obtained and the particle size was determined to be 3.60 and 3.68 µm respectively. Table 2 shows the particle size (d_{50}) for x=0 sample after pechini method and after ball milling for 2, 8, 16 and 40 h.

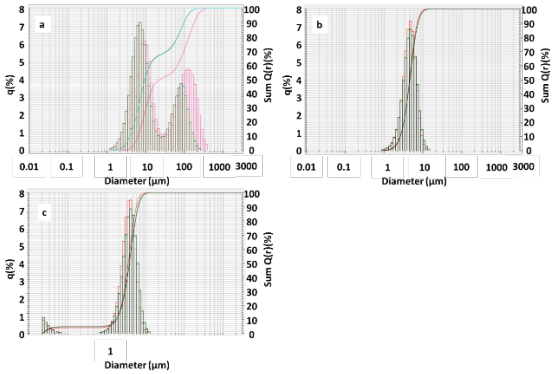

Fig. 8 Particle size distribution of x=0 sample after a) pechini preparation, b) ball milling for 2 h and c) ball milling for 8 h.

Table 2

Particle size of x=0 sample after pechini method and after ball milling for 2, 8, 16 and 40h.

Ball milling time (h)	Particle size d_{50} (µm)
Without ball milling	9.55
2	4.6
8	3.86
16	3.60
40	3.68

3.4. Effect of sintering time and temperature

For the cathodes sintered at 850 °C (x=0.1-0.2 samples), it was found that as the sintering time increases (2, 3, 4 and 5 h), there is no noticeable change in the porosity observed for x=0.1 (Fig. 9 a, b, c and d) and also for x=0.2 sample. For the cathodes sintered at 900 °C (x=0-0.1A samples), it was found that as the sintering time increases (3, 4 and 5 h) there is no noticeable change in the porosity observed. Fig. 10 (a, b, c and d) shows the SEM images of the cross sections of cathodes sintered at 500 °C for 1 h and then for 3 h at 850 °C. Fig. 11 (a, b, c and d) shows the SEM images of the cross sections of cathodes sintered at 500 °C for 1h and then for 3h at 900 °C. For all the $Ca_3Co_{4-x}Cu_xO_9$ cathodes, the cathodes have homogeneous microstructure. The adhesion of the cathode on the anode supported cell is correct. In the mixed ionic and the electronic conductors, the electrode's reactivity could be improved by mixing the electrode material with the electrolyte material due to the expansion of a triple phase boundary (TPB) [22]. In this frame, composite cathodes are prepared and reported in Table 3 for studying the microstructure, homogeneity and the adhesion to an anode supported cell. From Fig.10 c and d and Fig.11 c, and d it is clear that all the composite cathodes have homogeneous microstructure. The contact of the cathode to the anode supported cell looks sufficient and it seems that GDC grains form a continuous network.

Table 3

Name, cathode composition and the thermal treatment for the prepared composite cathodes.

Name	Composition	Thermal treatment
$x_{0.1}$-GDC	50 wt% $Ca_3Co_{3.9}Cu_{0.1}O_9$-50 wt% $Gd_{0.2}Ce_{0.8}O_2$	500 for 1h and then 850 °C for 3 h
$x_{0.2}$-GDC	50wt % $Ca_3Co_{3.8}Cu_{0.2}O_9$-50 wt % $Gd_{0.2}Ce_{0.8}O_2$	500 for 1h and then 850 °C for 3 h
x_0-GDC	50wt% $Ca_3Co_4O_9$-50wt% $Gd_{0.2}Ce_{0.8}O_2$	500 for 1h and then 900 °C for 3 h
$x_{0.1A}$-GDC	50 wt% $Ca_3Co_{3.9}Cu_{0.1}O_9$-50 wt% $Gd_{0.2}Ce_{0.8}O_2$	500 for 1h and then 900 °C for 3 h

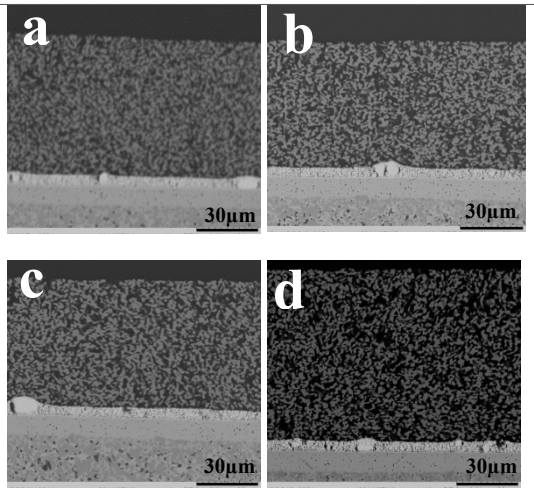

Fig. 9 SEM images of the cross sections of x=0.1 cathodes sintered at 850 °C for a)2 h, b)3 h, c)4 h and d)5 h.

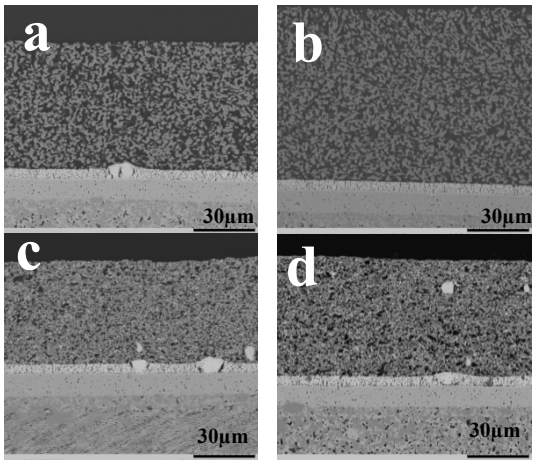

Fig. 10 SEM images of the cross sections of a) x=0.1, b) x=0.2, c) ($x_{0.1}$-GDC) and d) ($x_{0.2}$-GDC) cathodes sintered at 850 °C for 3 h.

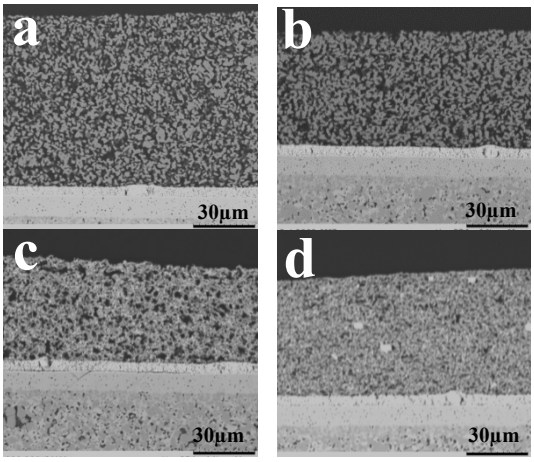

Fig. 11 SEM images of the cross sections of a) x=0, b) x=0.1, c) (x_0-GDC) and d) ($x_{0.1A}$-GDC) cathodes sintered at 900 °C for 3 h.

3.5. Electrochemical properties of Cu-CCO-GDC composite cathodes

For the electrochemical performance tests, symmetrical cells of $x_{0.1}$-GDC and $x_{0.2}$-GDC composite cathodes were screen printed on screen printed layer of GDC on dense 8 YSZ. The symmetrical cells were then sintered at 850 °C for 3h. The Fig. 12 shows the typical Nyquist plots of $x_{0.1}$-GDC and $x_{0.2}$-GDC composite cathodes in the temperature range of 600 to 800 °C in air. It is clear that as the temperature increases the overall size of the impedance arcs decreased for both composite cathodes. Fig 13 shows the ASR and the ohmic resistance for the two composite cathodes as a function of temperature in the temperature range from 600 to 800 °C. It is clear that the area specific resistance (ASR) for $x_{0.2}$-GDC composite cathode is lower than that of $x_{0.1}$-GDC. The electrochemical performance of the $x_{0.2}$-GDC composite cathode is better than that of $x_{0.1}$-GDC composite cathode. This might be due to its relatively better catalytic activity and electrical conductivity. The ohmic resistance of $x_{0.1}$-GDC is high. This might be due to delamination or presence of secondary phases.

At 700 °C, the ASR of $x_{0.2}$-GDC is less than 0.5 Ω cm^2 which is less than the ASR value (about 1Ω cm^2) of hand painted 70 wt% CCO-30 wt % GDC composite cathode prepared by Nagasawa et al [6], the ASR values (4.5 Ω cm^2 and 1.5 Ω cm^2) of screen printed 70 wt% CCO-30 wt % GDC composite cathode with different thickness (5µm and 20µm) prepared by Aurelie et al [18] and the ASR values for 30 wt % SDC-70 wt % CCO-Bi0.1 (1.39 Ω cm^2) [22]. Reduction of the ASR value of $x_{0.2}$-GDC might be attributed to the reduction of the resistivity due to the substitution of Co ions by Cu ions [30] in addition to the thickness and the composition of $x_{0.2}$-GDC composite cathode. $x_{0.1}$-GDC is comparable to the previous reported work.

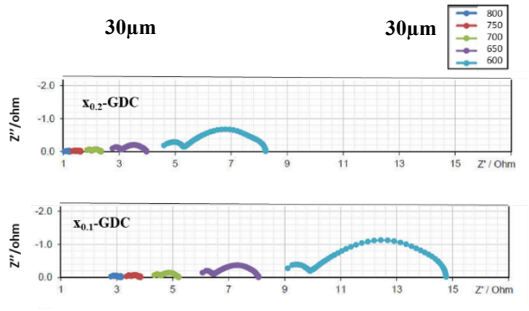

Fig. 12 The impedance spectra of $x_{0.1}$-GDC and $x_{0.2}$-GDC cathodes in air in the temperature range 600-800 °C.

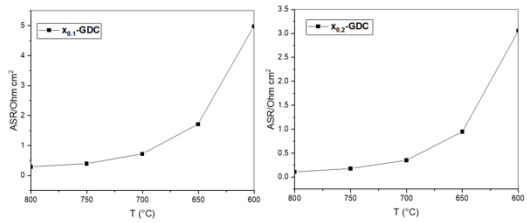

Fig. 13 The ASR and ohmic resistances for $x_{0.1}$-GDC and $x_{0.2}$-GDC cathodes in air in the temperature range 600-800 °C.

4. Conclusion

The Pechini method was used for the preparation of $Ca_3Co_{4-x}Cu_xO_9$ powders where x= 0, 0.1, 0.2 and 0.3 with the particular intention of studying the CuO concentration effect on the structural properties, sinterability, and electrochemical performance. All the prepared samples have only the monoclinic phase reported for $Ca_3Co_4O_9$ (CCO) except the $Ca_3Co_{3.7}Cu_{0.3}O_9$ sample have additionally secondary phase as minor. Cu doping improved the sinterability of $Ca_3Co_4O_9$. From SEM, all the studied electrodes have a homogeneous microstructure, acceptable porosity and correct adhesion with the anode supported cell. The $x_{0.2}$-GDC composite cathode is better than that of $x_{0.1}$-GDC composite cathode.

Conflict of Interest

There is no conflict of interest.

Acknowledgments

The author is grateful to thank Forschungszentrum Jülich GmbH, Institute of Energy and Climate Research, IEK-1: Materials Synthesis and Processing, 52425 Jülich, Germany Also the author is grateful to thank Prof. Dr. I. A. Farag and Prof. Dr A. A. Ramadan for their help in the investigation of the dilatometry part. The author also is grateful to thank Prof. Dr. Ahmed Hashim and Prof. Dr. Ashraf Abdel-Ghany for their fruitful and strong support.

References

[1] O. Celikbilek, C.-A. Thieu, F. Agnese, E. Calì, C. Lenser, N.H. Menzler, J.-W. Son, S.J. Skinner, E. Djurado, Enhanced catalytic activity of nanostructured, A-site deficient (La0. 7Sr0. 3) 0.95 (Co0. 2Fe0. 8) O3− δ for SOFC cathodes, J. Mater. Chem. A. 7 (2019) 25102–25111.

[2] J. Zhang, C. Lenser, N.H. Menzler, O. Guillon, Comparison of solid oxide fuel cell (SOFC) electrolyte materials for operation at 500 C, Solid State Ionics. 344 (2020) 115138.

[3] J. Zhang, C. Lenser, N. Russner, A. Weber, N.H. Menzler, O. Guillon, Boosting intermediate temperature performance of solid oxide fuel cells via a tri-layer ceria–zirconia–ceria electrolyte, J. Am. Ceram. Soc. (2022).

[4] G. Yang, C. Su, H. Shi, Y. Zhu, Y. Song, W. Zhou, Z. Shao, Toward reducing the operation temperature of solid oxide fuel cells: our past 15 years of efforts in cathode development, Energy & Fuels. 34 (2020) 15169–15194.

[5] S.B. Adler, Factors governing oxygen reduction in solid oxide fuel cell cathodes, Chem. Rev. 104 (2004) 4791–4844.

[6] K. Nagasawa, S. Daviero-Minaud, N. Preux, A. Rolle, P. Roussel, H. Nakatsugawa, O. Mentré, Ca3Co4O9− δ: A thermoelectric material for SOFC cathode, Chem. Mater. 21 (2009) 4738–4745.

[7] K.-Y. Lai, A. Manthiram, Effects of trivalent dopants on phase stability and catalytic activity of YBaCo 4 O 7-based cathodes in solid oxide fuel cells, J. Mater. Chem. A. 6 (2018) 16412–16420.

[8] A. V Nikonov, K.A. Kuterbekov, K.Z. Bekmyrza, N.B. Pavzderin, A brief review of conductivity and thermal expansion of perovskite-related oxides for SOFC cathode, Eurasian J. Phys. Funct. Mater. 2 (2018) 274–292.

[9] A.J. Samson, M. Søgaard, N. Van Nong, N. Pryds, N. Bonanos, Enhanced electrochemical performance of the solid oxide fuel cell cathode using Ca3Co4O9+ δ, J. Power Sources. 196 (2011) 10606–10610.

[10] A. Sotelo, G. Constantinescu, S. Rasekh, M.A. Torres, J.C. Diez, M.A. Madre, Improvement of thermoelectric properties of Ca3Co4O9 using soft chemistry synthetic methods, J. Eur. Ceram. Soc. 32 (2012) 2415–2422.

[11] U. Hira, S.S. Ali, S. Latif, N. Pryds, F. Sher, Improved High-Temperature Thermoelectric Properties of Dual-Doped Ca3Co4O9, ACS Omega. 7 (2022) 6579–6590.

[12] Y.-N. Li, P. Wu, S.-P. Zhang, S. Chen, D. Yan, J.-G. Yang, L. Wang, X.-L. Huai, Thermoelectric properties of lower concentration K-doped Ca3Co4O9 ceramics, Chinese Phys. B. 27 (2018) 57201.

[13] Y. Fan, X. Qing, D. Zeng, Effect of Y doping at Co site on thermoelectric properties of Ca3Co4O9, Funct. Mater. Lett. 13 (2020) 2051009.

[14] X.-L. Tang, Z.-H. Ge, Z. Li, K. Zhao, Enhanced thermoelectric properties of Ca3Co4O9+ δ ceramics by Sr substitution, Solid State Sci. 104 (2020) 106190.

[15] B. Özkurt, M.E. Aytekin, M.A. Madre, A. Sotelo, M.A. Torres, Improving thermoelectric properties of Ca3Co4O9+ δ through both Na doping and K addition at optimal values, J. Mater. Sci. Mater. Electron. 30 (2019) 8832–8837.

[16] U. Hira, L. Han, K. Norrman, D.V. Christensen, N. Pryds, F. Sher, High-temperature thermoelectric properties of Na- and W-doped Ca 3 Co 4 O 9 system, RSC Adv. 8 (2018) 12211–12221.

[17] C.O. Romo de la Cruz, Enhancing the Thermoelectric Performance of Calcium Cobaltite Ca3Co4O9 through Single and Dual Elements Doping, (2019).

[18] A. Rolle, S. Boulfrad, K. Nagasawa, H. Nakatsugawa, O. Mentré, J. Irvine, S. Daviero-Minaud, Optimisation of the solid oxide fuel cell (SOFC) cathode material Ca3Co4O9− δ, J. Power Sources. 196 (2011) 7328–7332.

[19] A. Rolle, V. Thoréton, P. Rozier, E. Capoen, O. Mentré, B. Boukamp, S. Daviero-Minaud, Evidence of the current collector effect: study of the SOFC cathode material Ca3Co4O9+ δ, Fuel Cells. 12 (2012) 288–301.

[20] H. Ben Yahia, F. Mauvy, J.C. Grenier, Ca3− xLaxCo4O9+ δ (x= 0, 0.3): New cobaltite materials as cathodes for proton conducting solid oxide fuel cell, J. Solid State Chem. 183 (2010) 527–531.

[21] J. Zou, J. Park, H. Yoon, T. Kim, J. Chung, Preparation and evaluation of Ca3− xBixCo4O9− δ (0< x≤ 0.5) as novel cathodes

for intermediate temperature-solid oxide fuel cells, Int. J. Hydrogen Energy. 37 (2012) 8592–8602.
[22] J. Zou, J. Park, H. Yoon, N.M. Sammes, J. Chung, Effects of transition metal ion dopants on the performance of Ca2. 9Bi0. 1Co4O9− δ cathode, J. Alloys Compd. 558 (2013) 188–194.
[23] P. Guo, X. Huang, X. Zhu, Z. Lü, Y. Zhou, L. Li, Z. Li, B. Wei, Y. Zhang, W. Su, A New Composite Material Ca3Co4O9+ δ+ La0. 7Sr0. 3CoO3 Developed for Intermediate-Temperature SOFC Cathode, Fuel Cells. 13 (2013) 666–672.
[24] V. Thoréton, Y. Hu, C. Pirovano, E. Capoen, N. Nuns, A.S. Mamede, G. Dezanneau, C.Y. Yoo, H.J.M. Bouwmeester, R.N. Vannier, Oxygen transport kinetics of the misfit layered oxide Ca 3 Co 4 O 9+ δ, J. Mater. Chem. A. 2 (2014) 19717–19725.
[25] S.-F. Wang, Y.-F. Hsu, J.-H. Chang, S. Cheng, H.-C. Lu, Characteristics of Cu and Mo-doped Ca3Co4O9− δ cathode materials for use in solid oxide fuel cells, Ceram. Int. 42 (2016) 11239–11247.
[26] A. Rolle, H.A.A. Mohamed, D. Huo, E. Capoen, O. Mentre, R.-N. Vannier, S. Daviero-Minaud, B.A. Boukamp, Ca3Co4O9+ δ, a growing potential SOFC cathode material: impact of the layer composition and thickness on the electrochemical properties, Solid State Ionics. 294 (2016) 21–30.
[27] E. Djurado, A. Salaün, G. Mignardi, A. Rolle, M. Burriel, S. Daviero-Minaud, R.-N. Vannier, Electrostatic spray deposition of Ca3Co4O9+ δ layers to be used as cathode materials for IT-SOFC, Solid State Ionics. 286 (2016) 102–110.
[28] X. Zhu, A. Lusi, C. Zhu, Y. Wang, J. Jin, Performance evaluation of Ca3Co4O9-δ cathode on Sm0. 075Nd0. 075Ce0. 85O2-δ electrolyte for solid oxide fuel cells, J. Alloys Compd. 694 (2017) 877–883.
[29] Y. Huang, B. Zhao, X. Hu, S. Lin, R. Ang, W. Song, Y. Sun, Enhanced electronic correlation and thermoelectric response by Cu-doping in Ca 3 Co 4 O 9 single crystals, Dalt. Trans. 41 (2012) 11176–11186.
[30] Y. Wang, Y. Sui, P. Ren, L. Wang, X. Wang, W. Su, H. Fan, Strongly correlated properties and enhanced thermoelectric response in Ca3Co4− x M x O9 (M= Fe, Mn, and Cu), Chem. Mater. 22 (2010) 1155–1163.
[31] S. Rasekh, M.A. Torres, G. Constantinescu, M.A. Madre, J.C. Diez, A. Sotelo, Effect of Cu by Co substitution on Ca3Co4O9 thermoelectric ceramics, J. Mater. Sci. Mater. Electron. 24 (2013) 2309–2314.
[32] X.R. Liu, S.Y. Li, Y. He, Y. Lu, Y.R. Jin, N.B. Feng, Thermoelectric properties of 0.7 Ca 3 Co 4− x Cu x O 9/0.3 Bi 2 Ca 2 Co 2− z Cu z O y (x= 0, 0.05, 0.1; z= 0, 0.05, 0.1) composites, J. Mater. Sci. Mater. Electron. 28 (2017) 13414–13419.
[33] M.P. Pechini, Method of preparing lead and alkaline earth titanates and niobates and coating method using the same to form a capacitor, 1967.
[34] H.A. Abbas, R.A. Nasr, A. Khalaf, A. Al Bawab, T.S. Jamil, Photocatalytic degradation of methylene blue dye by fluorite type Fe2Zr2-xWxO7 system under visible light irradiation, Ecotoxicol. Environ. Saf. 196 (2020) 110518.
[35] H.A. Abbas, R.A. Nasr, R.N. Vannier, T.S. Jamil, Improving of photocatalytic activity of barium ferrate via bismuth and copper co-doping for degradation of paracetamol under visible light irradiation, J. Environ. Sci. 112 (2022) 331–342. https://doi.org/10.1016/J.JES.2021.05.008.
[36] A. Bhaskar, Y.C. Huang, C.-J. Liu, Thermoelectric properties of Ca3− xEuxCo4O9+ δ (0≤ x≤ 0.1), Solid State Commun. 168 (2013) 24–27.
[37] L. Xu, F. Li, Y. Wang, High-temperature transport and thermoelectric properties of Ca3Co4− xTixO9, J. Alloys Compd. 501 (2010) 115–119.
[38] T. Oide, Y.; Miyazaki, Y.; Huang, X. Y.; Kajitani, Proceedings of XXV International Conference on Thermoelectrics (ICT ’06), in: Proc. XXV Int. Conf. Thermoelectr. (ICT ’06), New York, Vienna, Austria, 2006: pp. 402–405.